Development of New Double-Stranded Phenylalanyl Chelators Using η–χ Diagrams and Binding Constants for Chelators and Lanthanide Ions

Shigeki KOBAYASHI,* Makoto WATANABE, and Toshiyuki CHIKUMA

Department of Analytical Chemistry of Medicines, Showa Pharmaceutical University; 3–3165 Higashi-tamagawagakuen, Machida, Tokyo 194–8543, Japan.

Received October 2, 2009; accepted February 6, 2010; published online February 15, 2010

We examined the interaction between several ligands and alkaline (M^+) or lanthanide (Ln^{3+}) ions using η–χ diagrams. η and χ represent absolute hardness and absolute electronegativity, respectively. Based on the diagrams, new double-stranded amino acid chelators (1) conjugated to Cat (catechol) were synthesized. They had two cavities coordinating hard metal ions, such as Li^+ and K^+, and soft metal ions, such as Lu^{3+} and Eu^{3+}. 1 formed a solvated molecular complex, 1–Ln^{3+}, with a molar ratio of 1 : 1 at a binding constant (K_b) of 10^4—10^6 with Y^{3+}, La^{3+}, Eu^{3+}, and Lu^{3+}, respectively. With a chemical hard ion, Li^+, we found that the K_b of the 1–Eu^{3+} complex increased. The optimized geometries of 1–Lu^{3+} and 1–La^{3+} complexes were obtained from B3LYP correlation functions using Stuttgart-Dresden-Bonn (SDD) Effective Core Potential (ECP) basis sets for Lu^{3+} and La^{3+} ions. The double-stranded chelator may prove useful for studying the selective separation of lanthanide ions, and the development of functional peptides.

Key words chemical hardness; double-stranded amino acid; chelator; lanthanide ion; binding constant

Lanthanides (Ln) as heavy rare earth elements and Y are attracting the interest of chemists since complexes prepared by the reaction of lanthanide ions (Ln^{3+}) with chelators have a variety of applications, including probes for fluorometry,[1—4] catalysts,[5] sensitizing chromophores,[6—8] and nanomaterials.[9,10] Recently, lanthanide ions with unique photophysical and coordination properties have been used to develop lanthanide-antenna sensors as luminescent sensors for cellular imaging,[8] and protein and DNA assays. As chemical and physicochemical properties, lanthanides are chemically similar to metal ions because of the shielding of progressively filled inner 4*f* orbitals by the filled outer 5*s* and 5*p* orbitals and the lanthanide contraction effect. The study of the stability of lanthanide-ligand complexes is interesting because the lanthanide contraction effect appears to vary directly with the ionic radius.

The development of chelator–Ln^{3+} complexes has been of interest to investigators of the regioselective lanthanide-induced hydrolysis of phosphate esters, including DNA and RNA.[11] Such compounds are potentially applicable to pharmacological fields[12] as chemotherapeutic agents, such as the platinum anticancer drug cisplatin. Generally, chelator–Ln^{n+} complexes have low solubility. The design of chelators, which have both hydrophobic parts (or regions) and hydrophilic parts in the same molecule, is required to increase the solubility of Ln^{n+} ions. We envisage the development of highly soluble chelator–Ln^{n+} complexes which express biological effects through coordination with the binding sites of drugs, proteins, and DNA. It is necessary to understand which ligands coordinate easily with Ln^{3+}; however, there is no convenient chemical method of examining the interaction between chelators and metal ions.

In the past several years, the development of theoretical models of metals and molecules based on electrophilicity (ω) and chemical hardness (η) indexes for the characterization of chemical reactions, biological activity, and atoms has progressed steadily.[13] The concepts of chemical hardness, absolute hardness [$\eta = 1/2(\partial^2 E/\partial N^2)$] and absolute electronegativity [$\chi = -(\partial E/\partial N)$],[14,15] which have been associated with the theory of chemical reactivity in molecules, are being applied to the design of chelators and chemicals.[16,17] N is the total electron number and E is total electron energy.

To develop chelators, we have focused on a convenient model using quantum chemical η–χ diagrams for chelators and lanthanide ions based on the chemical hardness concept, η and χ, as described above. The η–χ diagram shows that phenol and Cat (catechol) are appropriate for the reaction of a ligand with Ln^{n+} ions since Ln^{n+} is chemically harder than phenol and Cat.

Here, we report a new chelator (**1**) that conjugated Cat to bis(*tert*-butoxycarbonyl (Boc)-L-Phe)-*N*,*N*-ethylenedioxy-bis(ethylamine), which should support a β-sheet-like conformation.[18,19] The chelator could expect flexible conformation due to a backbone conjugated with two amino acid residues to the N-terminus of a spacer, –O–CH_2–CH_2–O–, and its binding site is Cat, not an amido group. Chelator **1** provides a coordinate bond complex with Ln^{3+} of the largest ionic radius in 10 mM *N*-(2-hydroxyethyl)piperazine-*N*′-(2-ethanesulfonic acid) (HEPES) buffer in 70% MeCN (pH 4.8). Indeed, the binding constants of **1**–Ln^{3+} complexes are about 10^4—10^6 M^{-1}. Therefore, we show that compound **1** analogs with ligand Cat are excellent chelators for Ln^{3+}. Complexes of chelator **1** with Ln^{3+} may be applied in the pharmacological field as chemotherapeutic agents and luminescent sensors,[8] which are a subject of many recent studies.

In addition, the quantum chemical η–χ diagram is a useful tool for the design of chelators, and we will deal with the synthesis and characterization of the complexes of the chelator with Ln^{3+}. To rationalize the structure of chelator–Ln^{n+} complexes, we also discussed the structural properties of complexes of the chelator with La^{3+} and Lu^{3+} using the B3LYP level.

Results and Discussion

Design of an Active Site: Quantum Chemical η–χ Diagrams for Lanthanide Ions The relation between the ionization potential (I*p*) and electron affinity (E*a*) of metal ions (M^{n+}) is shown in Eq. 1. The values of absolute hardness (η)

* To whom correspondence should be addressed. e-mail: kobayasi@ac.shoyaku.ac.jp

and absolute electronegativity (χ) were calculated using data published previously.[20)]

Coordinate $\mathbf{r}(\chi, \eta)$ as the electronic structure of Ln^{3+} was calculated from Eqs. 1, 2, and 3.

$$Ln^{3+}: Ln^{3+}(Ea) \rightarrow Ln^{4+}(Ip) + e^- \quad (1)$$

$$-\mu = \frac{(Ip + Ea)}{2} = \chi \quad (2)$$

$$\eta = \frac{(Ip - Ea)}{2} \quad (3)$$

Where μ is chemical potential. Here, we found that the $\mathbf{r}(\chi, \eta)$ of lanthanide ions, Ln^{3+}, having 4*f* electrons, has no linear relationship between absolute hardness and absolute electronegativity. In the diagram of $\mathbf{r}(\chi, \eta)$, Sc^{3+} (4*f*=0), Y^{3+} (4*f*=0), La^{3+} (4*f*=0), and Gd^{3+} (4*f*=7) have a two-order correlation between η and χ, and we found that the correlation curve was fitted with $\eta = -0.0308\chi^2 + 3.2518\chi - 61.171$ (correlation coefficient (*r*): *r*=0.9994); however, Ce^{3+} (4*f*=1)–Eu^{3+} (4*f*=6) and Dy^{3+} (4*f*=9)–Lu^{3+} (4*f*=14) groups did not show a linear relationship between η and χ (Fig. 1). The graph has no two-order or three-order correlations; however, the behavior of Gd^{3+} is similar to that of Sc^{3+}, Y^{3+}, and La^{3+} although it has 4*f* electrons. This may be explained by the relativity theory for heavy rare earth elements.[21)]

Hughes *et al.* reported that although the effects of spin orbital coupling of Gd^{3+} can be neglected, the spin orbital coupling and orbital moments of other Ln^{3+} ions with 4*f* electrons are important to obtain estimates of magnetic moments and magnetic ordering temperatures.[22)] Therefore, heavy rare earth elements and related elements, Sc^{3+}, Y^{3+}, La^{3+}, and Gd^{3+}, which can be neglected in terms of the effect of relativity theory, are determined using the $\mathbf{r}(\chi, \eta)$ diagram. For example, the η of Ce^{3+} is 8.28 and that of Gd^{3+} is 11.71. Ce^{3+} is chemically softer and Gd^{3+} is harder than other Ln^{3+} ions with 4*f* electrons. The η of lanthanum ions, La^{3+}, is 14.875 and La^{3+} lack three electrons, $(5d)^1(6s)^2$, since the electron configuration of a neutral La is $(4d)^{10}(4f)^0(5s)^2(5p)^6$. Eu^{3+} has the electron configuration $(4d)^{10}(4f)^6(5s)^2(5p)^6$.

To achieve the design and synthesis of functional chelators, which selectively bind with chemically soft Eu^{3+} and Eu^{3+} ions, we discuss a method for the development of chelators using $\mathbf{r}(\chi, \eta)$ diagrams of Ln^{3+} ions and ligands (L) (**2**—**10**). As a soft-based chelator is favorable for binding soft-acid metal M^{n+} ions according to the hardness concept, our target is a chemically soft ligand. In addition, our aim is to design a L–Ln^{3+} complex in which the binding force between the ligand and M^{n+} ion is weak; that is, ligand exchange is active. The interaction of Ln^{3+} ions with the ligand as a donor is a result of an overlap of orbitals or of electrostatic binding of two Ln^{3+} ions and L (Eq. 4).

$$\underset{\text{(ligand)}}{L} + Ln^{3+} \rightleftarrows L\text{–}Ln^{3+} \quad (4)$$

We show a $\mathbf{r}(\chi, \eta)$ diagram plotting the η and χ of several ligands calculated using the density functional theory B3LYP with a 6-31G(*d*) basis set (Fig. 1). When Ln^{3+} forms a complex with L, electrons flow from L to Ln^{3+}. The quantitative charge transfer (ΔQ) and stabilization energy (ΔE) were calculated using Eqs. 5 and 6.[14)]

$$\Delta Q = \frac{(L\text{–}Ln^{3+})}{2(L\text{–}Ln^{3+})} \quad (5)$$

$$\Delta E = -\frac{(L\text{–}Ln^{3+})^2}{4(L\text{–}Ln^{3+})} \quad (6)$$

According to Eqs. 5 and 6, the softer the target chelator, the less favorably it binds with Ln^{3+} ions. In the diagram in Fig. 1a, the Cat (**7**) is a softer chelator than 18-crown-6-ether (**2**), en (**3**), ethylenediaminetetraacetic acid (EDTA) (**4**), 12-ane-4 (**5**), and calixarene (**8**), and the χ of Cat is smaller than that of **3**, **4**, or **5**. In making up the electrostatic Cat–Eu^{3+} complex of Cat with Eu^{3+}, the stabilization energy ΔE is −20.48 (eV), as listed in Table 1. The value is larger than that of **2**—**6** and **8**—**10**. These values are expressed as the binding force of the chelators with La^{3+} and Eu^{3+} ions. Moreover, the ΔQ of the **7**–Eu^{3+} complex is −1.317. This indicates that electrons easily withdraw Eu^{3+} from **7**. Calculated ΔQ and ΔE values indicate that the stabilization of ligand–Eu^{3+} complexes decreases in the following order: **7**–Eu^{3+}>**8**–Eu^{3+}>**10**–Eu^{3+}>**9**–Eu^{3+}>**6**–Eu^{3+}>**3**–Eu^{3+}>**4**–Eu^{3+}>**5**–Eu^{3+} and >**2**–Eu^{3+} (Table 1). This indicates that ligand **6** would form a stable solvated complex with Ln^{3+} ions in solution; therefore, we designed and synthesized a novel chelator (**1**), in which a chemically soft ligand **7** was conjugated to two terminals in the molecule. Although the spacer –HN–CH_2CH_2–O–CH_2CH_2–O–CH_2CH_2–NH– of **1** is as chemically hard as ligand **2** or **5**, **1** joined to **7** is a chemi-

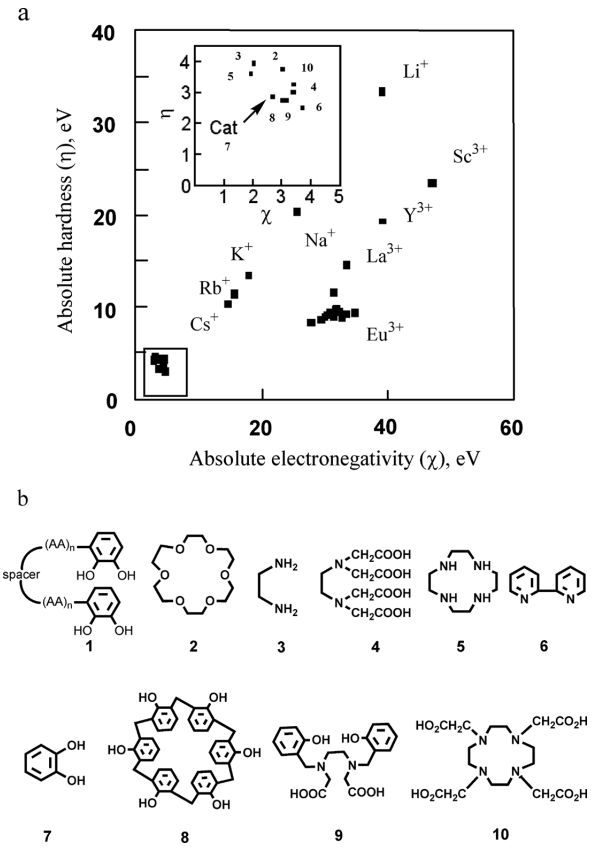

Fig. 1. Plot of $\mathbf{r}(\chi, \eta)$ as a Coordinate Diagram of Electronic Structure for Alkaline (M^+) and Lanthanide Ions (Ln^{3+}) (a), and Structures of Several Chelators (**2**—**10**) (b)

(a) Data of I*p* and E*a* for alkaline and lanthanide ions were from ref. 20. (b) Upper square figure is enlarged the small square figure at the bottom left in Fig. 1a. Symbol AA is amino acid residues.

Table 1. Calculated Hardness (η), Electronegativity (χ), Quantitative of Charge Transfer (ΔQ) and Stabilization Energy (ΔE) for Chelators and Chelator–Ln^{3+} Complexes

Chelator	ε_{homo} [a] (eV)	ε_{lumo} [a] (eV)	η [a] (eV)	χ [a] (eV)	ΔQ La^{3+} [b] complex (eV)	ΔE La^{3+} [b] complex (eV)	ΔQ Eu^{3+} [b] complex (eV)	ΔE Eu^{3+} [b] complex (eV)
2	−6.973	0.8475	3.910	3.063	−0.839	−13.21	−1.201	−18.47
3	−6.152	2.192	4.172	1.980	−0.855	−13.94	−1.218	−19.39
4	−6.609	−0.4355	3.087	3.522	−0.864	−13.41	−1.264	−19.15
5	−5.602	1.916	3.759	1.843	−0.878	−14.37	−1.264	−20.20
6	−6.357	−1.318	2.520	3.837	−0.883	−13.57	−1.314	−19.68
7	−5.625	0.2195	2.922	2.703	−0.895	−14.26	−1.317	−20.48
8	−5.848	−0.2788	2.784	3.063	−0.892	−14.05	−1.317	−20.24
9	−6.066	−0.4787	2.794	3.272	−0.886	−13.86	−1.307	−19.95
10	−6.899	−0.1650	3.367	3.532	−0.851	−13.20	−1.235	−18.70

a) At the B3LYP/6-31G(*d*) level. *b*) Coordinate **r**(χ, η) of electronic state of La^{3+} and Eu^{3+} is **r**(34.57, 14.88) and **r**(33.81, 8.89), respectively.

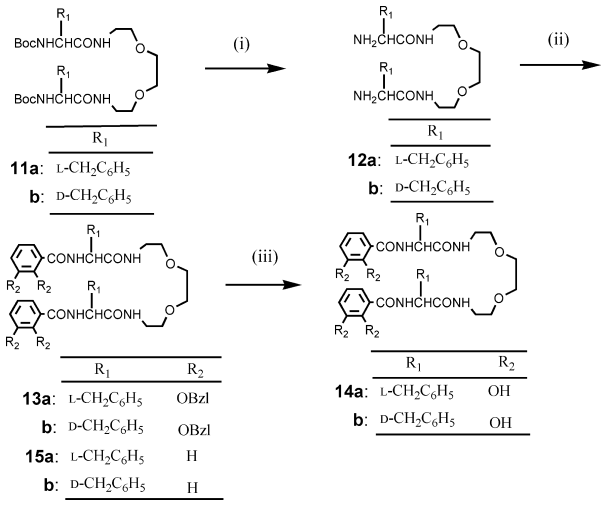

Fig. 2. Synthesis of Several Double-Stranded Amino Acid Chelators

Keys: (i) 90% TFA at 4 °C. (ii) Cat, DEPC, and TEA in dry DMF. (iii) 5% Pd/C–H_2 in MeOH.

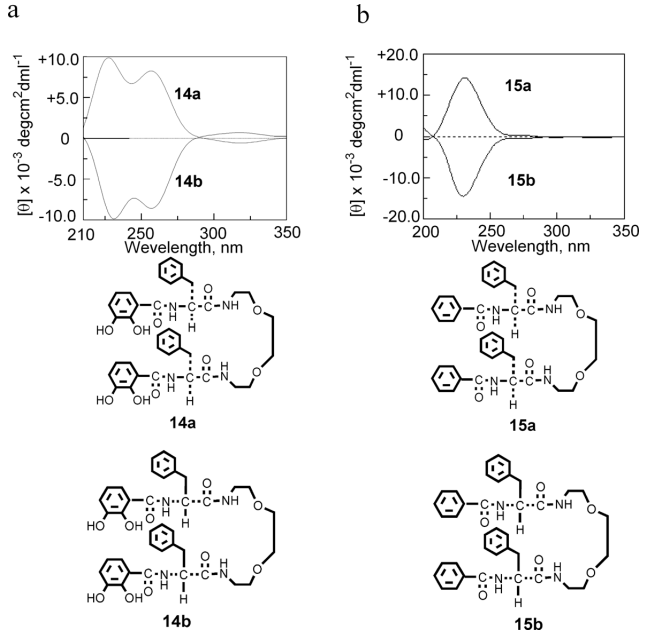

Fig. 3. Circular Dichroism Spectra of Double-Stranded Chelators

Circular dichroism spectra of (a) **14a**, **b** and (b) **15a**, **b** in 70% CH_3CN (10 mM HEPES buffer, pH 4.8) at 23±0.1 °C. Concentration of **14a**, **b** and **15a**, **b**: 1.50×10^{-4} M.

cally softer chelator than **7** or **8**.

Synthesis and Chemical Properties The synthesis of the target double-stranded amino acid chelators is shown in Fig. 2. Boc-L-Phe-OH was conjugated to 1,8-(ethylenedioxy)bis(ethylamine) to yield a Boc-protected bis(Boc-L-Phe)-*N*,*N*-(ethylenedioxy)bis(ethylamine) (**11a**) and **11a** was purified using silica gel chromatography with $CHCl_3$ and 3% MeOH/$CHCl_3$. Removal of the Boc groups by trifluoroacetic acid (TFA) afforded the free compound (**12a**) in good yield.[16,19] Conjugated 2,3-bis(benzyloxy)benzoic acid was prepared from 2,3-dihydroxybenzoic acid,[16] with the N-terminal of **12a** afforded by treatment with DEPC (phosphorocyanidate) on dry *N*,*N*-dimethylformamide (DMF). Deprotection of the Bzl (benzyl) group in **13a** using 5% Pd/C–H_2 gave a new peptide chelator (**14a**) in 65% yield. Both compounds, **14a** and **14b**, gave satisfactory results in IR, ^{1}H-NMR, ^{13}C-NMR, ^{1}H–^{1}H correlation spectroscopy (COSY), ^{13}C–^{1}H COSY NMR, and FAB-MS analyses.

The αH-1 of **14a** observed at 4.82 ppm in $CDCl_3$–DMSO-d_6 (volume ratio; 0.5/0.2) is coupled with an amido proton (–NH_bCO–) of 8.48 ppm and the observed $^3J_{\alpha,NH}$ is 7.9 Hz. The value indicates that **12a** has a β-sheet (7.0—10.0 Hz)-like conformation. The observed $^3J_{\alpha,NH}$ value of αH-1 of **15a** conjugated with benzoic acid is 8.0 Hz, which is also an acceptable coupling constant for a β-sheet-like conformation. Figures 3a and b show circular dichroism (CD) spectra of **14a**, **b** and **15a**, **b** in 70% CH_3CN (10 mM HEPES, pH 4.8) at 23±0.1 °C, and support that these are pure optical isomers. The CD curve of **14a** is obviously a mirror image of that of **14b**, and the intensity of mole ellipticity ([θ]) is equal to that of **14b** (Fig. 3a). Two positive and negative bands of CD of **14b** (or **14a**) at 234 and 257 nm are observed. In contrast, the CD band at 257 nm was not observed in **15a** (or **15b**)-conjugated nonphenolic benzoic acid or **15a** (or **15b**) (Fig. 3b); therefore, a second cotton effect of **14a** (or **14b**) at 257 nm was assigned in conjugated catecholic OH groups.

Determination of Binding Constants To characterize the ability of synthesized chelators to form complexes with lanthanides ions (Ln^{3+}), the binding constant (K_b), molar ratio (n : m) of the complex, and molar absorbance coefficient (ε) were obtained from UV/Vis titration data in Benesi–

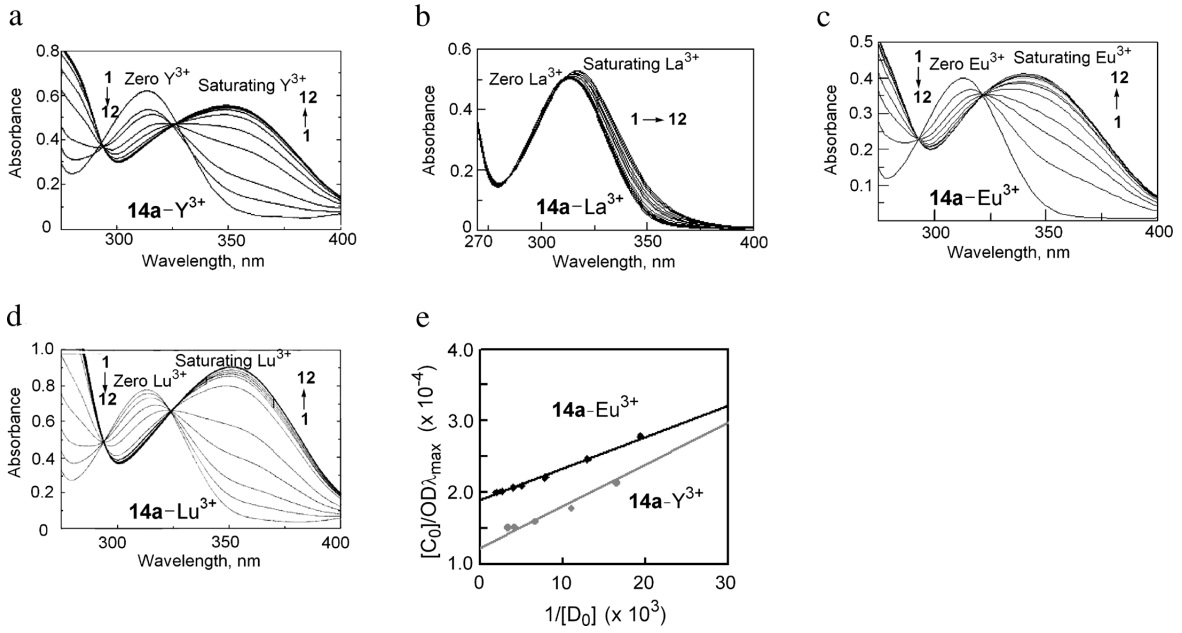

Fig. 4. UV/Vis Spectral Changes (a—d) of **14a** on the Addition of a Solution of Ln^{3+} and Benesi–Hildebrand Plots (e) on Complexation of **14a** with Lanthanide Ions Eu^{3+} and Y^{3+}

(a) **14a**–Y^{3+}, (b) **14a**–La^{3+}, (c) **14a**–Eu^{3+}, and (d) **14a**–Lu^{3+} complexes. Determination of the binding constant (K_{MY}) of **14a**–Eu^{3+} (λ_{max}=340 nm) and **14a**–Y^{3+} (λ_{max}=350 nm) complexes (e) with a Hildebrand plot.

Hildebrand plot analysis.[23] Figures 4a—d show the spectral change in UV/Vis titration studies on the binding of **14a** with Y^{3+}, La^{3+}, Eu^{3+}, or Lu^{3+}. UV/Vis spectra of the chelator **14a** were measured in 10 mM HEPES buffer in 70% MeCN (pH 4.8) and the first excited wavelength (λ_{max}) was 313 nm.

The absorbance of a colorless solution of **14a** at 313 nm decreased on the addition of Eu^{3+} from 2.60 to 129.0×10^{-5} M under a fixed concentration of **14a** (8.067×10^{-5} M). However, the absorbance of the new wavelength of the **14a**–Eu^{3+} complex at 340 nm (λ_{max}) increased on the addition of Eu^{3+} (Fig. 4c). As the **14a**–Eu^{3+} complex has a 1 : 1 molar ratio, the 1 : 1 binding constant (K_{MY}) of **14** for Ln^{3+} is calculated from the Benesi–Hildebrand plot. A charge in absorbance (OD_i) is only induced by the formation of a 1 : 1 complex between **14** ($[C_0]$, M) and Ln^{3+} ion ($[D_i]$, M), and the OD intensity (OD_i) at maximum wavelength (λ_{max}, 340 nm when **14a**) can be expressed by the following equations:

$$\frac{[C_0]}{OD_i} = \frac{1}{[D_i]\cdot K_{MY}\cdot\Delta\varepsilon} + \frac{1}{\Delta\varepsilon} \quad (7)$$

$$\frac{1}{\Delta\varepsilon} = y\text{-intercept} \quad \text{and} \quad \frac{1}{\Delta\varepsilon\cdot K_{MY}} = \text{slope} \quad (8)$$

Figure 4e shows Benesi–Hildebrand plots of the absorbance at 350 nm or 340 nm as a function of Y^{3+} or Eu^{3+} concentrations at a fixed concentration of **14a** according to Eqs. 7 and 8. From the slope, the K_{MY} of the **14a**–Y^{3+} and **14a**–Eu^{3+} complexes was 2.12 and 4.37×10^4 M^{-1}, respectively. The binding constants of other complexes are shown in Fig. 5. Stabilization increases in the following order: **14a**–Lu^{3+}<**14a**–Eu^{2+}<**14a**–Y^{3+}<**14a**–Eu^{3+}<**14a**–La^{3+}. The result indicates that the K_{MY} value of the complex between **14a** and Ln^{3+} is about 10^4—10^6 M^{-1}, similar to that of Ln^{3+} with calix[6]arene analogs.[24] In order to compare the binding ability of the enantiomer **14b**–Eu^{3+} complex with

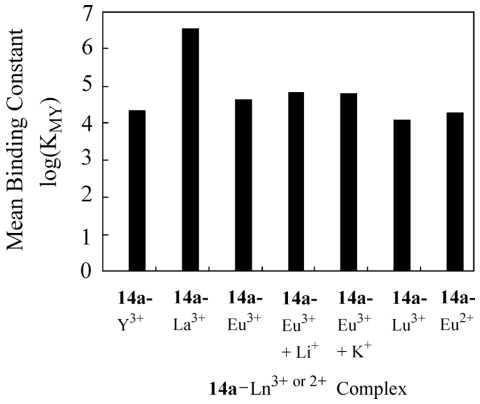

Fig. 5. Mean Binding Constant (K_{MY}) of Molecular Complexes Obtained from Spectrophotometric Titrations of Chelator **14a** with Lanthanide Ions

Each bar is the mean of two independent determinations at ≤±3% of the absolute errors.

the **14a**–Eu^{3+} complex, the binding constant $K_{\mathbf{14b}\text{–}Eu^{3+}}$ was measured by similar method: however, the $K_{\mathbf{14b}\text{–}Eu^{3+}}$ of D-form **14b** was almost the same value with L-form **14a**.

The shift of the second absorption from 313 to 317 nm of the complexes of **14a** with La^{3+} was much smaller than that of complexes of **14a** with Y^{3+} and Lu^{3+} (Figs. 4a, b, d). The K_{MY} of **14a**–La^{3+} is 3.43×10^6 M^{-1}, the largest in the Benesi–Hildebrand plot. Although the absorption shift of the **14a**–La^{3+} complex was small, the K_{MY} value was the largest in this study (Fig. 5). The λ_{max} of **14a**–Eu^{3+} (λ_{max} 340 nm) shifted to a larger value than that of chelator **14a** (λ_{max} 313 nm). The shifts of **14a**–Ln^{3+} complexes decreased in the following order: **14a**–Lu^{3+}>**14a**–Y^{3+}>**14a**–Eu^{3+}>**14a**–La^{3+}.

The reason for the difference in K_{MY}, for instance **14a**–Eu^{3+} and **14a**–La^{3+} complexes, is as follows. A large shift in λ_{max} indicates that the complex is polarized in the excited

state and ionizied; however, a small shift means that the complex is greatly polarized as in the case of the **14a**–La^{3+} complex. In the case of **14a**–Eu^{3+}, the large shift of λ_{max} in the excited state is associated with little polarization of the complex; therefore, **14a** and related chelators would be applicable to the separation of Ln^{3+} ions in solution. In addition, **14a** emits fluorescence with a λ^{em}_{max} of about 425 nm at λ^{ex}_{340} nm in 10 mM HEPES buffer in 70% MeCN (pH 4.8) (data not shown). Here, **15a** did not bind with the Ln^{3+} ions used in this study since the shift and increase in intensity at λ_{max} of the **15a**–Ln^{3+} complex was not observed by UV/Vis titration. This shows that catecholic ligands provide the function of **14**, not amide groups.

Molar Ratio and Structure The molar ratio of the complex between Ln^{3+} and the chelator was analyzed by continuous variation (a)[25] and molar ratio (b) methods (Figs. 6a, b).

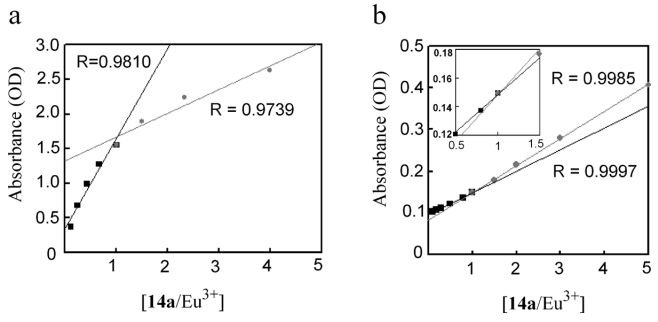

Fig. 6. Determination of Compositional Ratio of the **14a**–Eu^{3+} Complex with the Continuous Variation Method (a) and Molar Ratio Method (b)

(a) Ratio of [**14a**/Eu^{3+}]: 0.11, 0.25, 0.43, 0.67, 1.0, 1.5, 2.33, and 4.0; in 70% MeCN (10 mM HEPES, pH 4.8). (b) Ratio of [**14a**/Eu^{3+}]: 0.1, 0.2, 0.3, 0.5, 0.8, 1.0, 1.5, 2.0, 3.0 and 5.0; at λ=340 nm; in 70% MeCN (10 mM HEPES, pH 4.8). Concentration of **14a** and Eu^{3+}: 2.34×10^{-4} M and 1.17×10^{-5} M.

The continuous variation method gives the result for plots of [**14a**]/[Eu^{3+}] *vs.* absorbance. The molar ratio was the result for plots of [**14a**]/[Eu^{3+}] *vs.* absorbance for equilibrium under a fixed concentration of Eu^{3+} (1.17×10^{-5} M) at pH 4.8. With the continuous variation method (Fig. 6a), the plots gave two linear slopes in the ratio of concentration of [**14a**]/[Eu^{3+}]: $5.74\times10^{-5}/5.16\times10^{-4}$—$4.59\times10^{-4}/1.15\times10^{-4}$. It was found that the **14a**–Eu^{3+} complex has a 1 : 1 ratio since the intersection of the two slopes of correlation coefficient r=0.974 and 0.999 give a value of n/m=1 for altitude. Similar results were provided by the molar ratio method (Fig. 6b).

The molar ratio (**14a** : Eu^{3+} = 1 : 1) is useful to estimate the chemical structure of the **14a**–Ln^{3+} complex. Generally, Ln^{3+} ions yield complexes with coordination numbers of 8—12. To clarify the optimized structure satisfying conditions such as a 1 : 1 ratio and coordination number of 8, we estimated the optimized structure of **14a** (Fig. 7a) and the **14a**–La^{3+} complex (Fig. 7c) using the *ab initio* molecular orbital (MO) method. Figure 7 shows the results of B3LYP hybrid density functional methods with Stuttgart–Dresden–Bonn (SDD) effective core potentials (ECP)[26] basis set using the Gaussian 03 program[27]; however, the SDD ECP basis set was used for Ln^{3+} ions. C, H, N, and Cl atoms were optimized at the 6-31G(*d*) basis set level. The calculated mean O(4)–La^{3+} and HO(3)–La^{3+} bond lengths in the **14a**–La^{3+} complex are about 2.306 and 2.747 Å, respectively (Table 2), and the O–La^{3+} bond length is close to the observed length of the O–La^{3+} bond (2.443 Å) in TREN-1,2-HOIQO–La^{3+}.[28] The O(4)–Lu^{3+} bond length (2.202 Å) in the **14a**–Lu^{3+} complex is also similar to the observed length of the O–Lu^{3+} bond (2.287 Å) in the TREN-1,2-HOIQO–Lu^{3+} complex.[28] The results indicate that the structures of **14a**–La^{3+} and

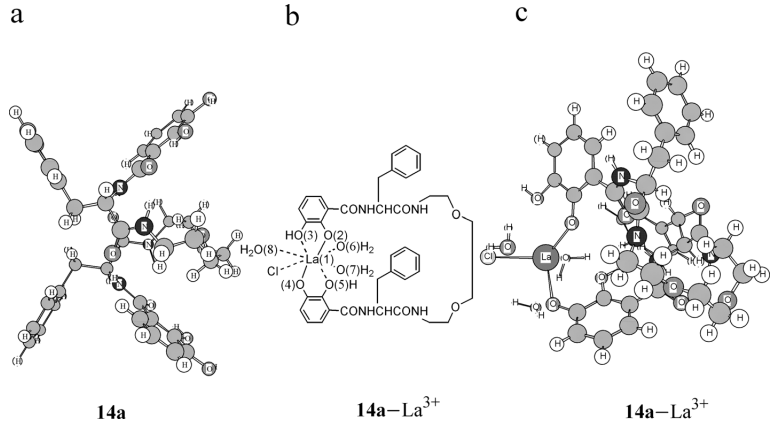

Fig. 7. Optimized Structure of **14a** and the **14a**–La^{3+} Complex

Structure of (a) **14a** and (c) the **14a**–La^{3+} complex shown as a ball and spoke model. At the B3LYP level using the SDD basis set for La, and an all-electron 6-31G(*d*) basis set for the remaining atoms.

Table 2. Calculated Bond Lengths, Dipole Moment, and Energies in Optimized Complexes of Chelator **14a** with Lanthanide Ions

	Energy (au)	Ln–O(2) (Å)	Ln–O(4) (Å)	Ln–O(3)H (Å)	Ln–O(5)H (Å)	Ln–Cl (Å)	Ln–O(6)H_2 (Å)	Ln–O(7)H_2 (Å)	Ln–O(8)H_2 (Å)	Dipole moment (debye)
14a[a]	−2444.671	—	—	—	—	—	—	—	—	1.433
14a–La^{3+}[b]	−3568.838	2.286	2.306	2.747	2.721	2.831	2.597	2.965	2.642	3.523
14a–Lu^{3+}[b]	−4369.489	2.144	2.202	2.433	2.471	2.670	2.355	2.513	2.418	2.634

a) At the B3LYP/6-31G(*d*) level. *b*) At B3LYP/6-31G(*d*), and SDD basis set was used for the optimization of La^{3+} and Lu^{3+}.

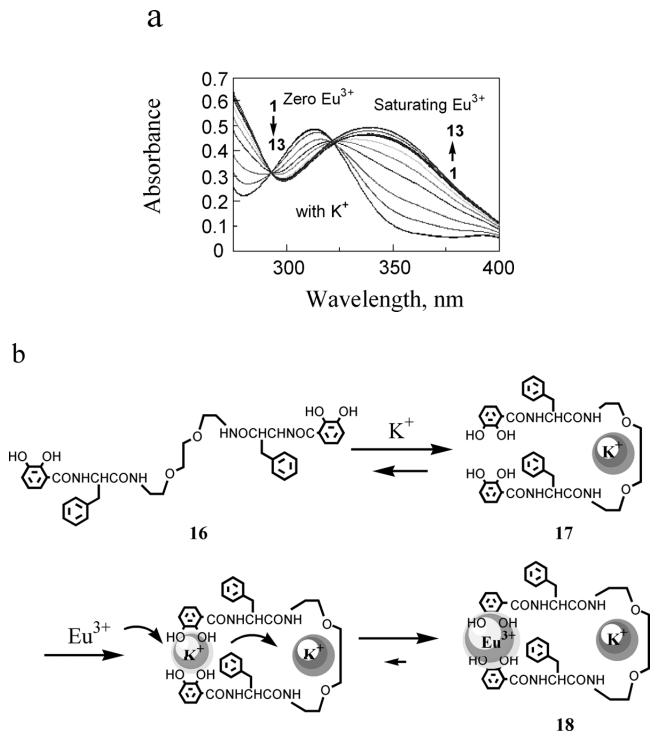

Fig. 8. Changes of UV Spectral Absorbance of (a) **14a** on Addition of Eu^{3+} with K^+ and (b) Folding Model of **14a** Bound with K^+ Ions

Arrow shows that hard K^+ moves into a hard base site from soft base Cat.

$-Lu^{3+}$ complexes are similar to the calculation results (Fig. 7c). In the **14a**–Lu^{3+} complex, the O(4)–Lu^{3+} bond length (2.202 Å) is about 0.104 Å shorter than that of **14a**–La^{3+}. The difference in length suggests an effect of the lanthanide contraction of Lu^{3+}. Spectrophotometric titration data show that the binding constant of the **14a**–Ln^{3+} complexes increases in the following order: **14a**–Lu^{3+}<**14a**–Eu^{2+}<**14a**–Y^{3+}<**14a**–Eu^{3+}<**14a**–La^{3+}, in the buffer (pH 4.8). Interestingly, this order may be identical to the order of the lanthanide contraction effect: $Lu^{3+}<Eu^{3+}<La^{3+}$ (Fig. 5).

The three mean H_2O–La^{3+} bond lengths in the **14a**–La^{3+} complex are 2.734 Å. The H_2O–La^{3+} bond length of the **14a**–La^{3+} complex increased about 0.305 Å more than the H_2O–Lu^{3+} bond of the **14a**–Lu^{3+} complex.

Effect of Hard Acid Li^+ and K^+ Ions Chemical soft and hard binding regions exist in **14**. Li^+ or K^+ ions are harder than Eu^{3+}, as shown in the η–χ diagram (Fig. 1a). In order to elucidate the effect of K^+ and Li^+ ions, UV/Vis titrations of **14a** with Eu^{3+} were performed in the presence of K^+ or Li^+ (7.70×10^{-5} M). Titration was performed at a molar ratio of 1 : 1 of [K^+]/[**14a**] in 10 mM HEPES buffer in 70% MeCN (pH 4.8) (Fig. 8a). The binding constant of the **14a**–Eu^{3+} complex with K^+ is 5.94×10^4 M^{-1}. The binding constant increased about 40% without K^+. In the presence of chemically harder Li^+, the binding constant of the **14a**–Eu^{3+} complex (6.71×10^4 M^{-1}) increased about 53.5% more than with K^+.

The increase in $K_{\mathbf{13a}\text{–}Eu^{3+}}$ may be explained by the illustration (Fig. 8b). First, equilibrium moves to the right with the coordination of K^+ (or Li^+) to a chemically hard base –O–CH_2CH_2–O– spacer of **14a**, which provides the folding conformation. The K^+–(–O–CH_2CH_2–O–) complex transforms the random conformation (**16**) to the folding conformation (**17**). Next, the chemically soft acid Eu^{3+} interacts with a chemically soft base, catecholic hydroxide of **14a**, and the complex (**18**) is stabilized by the valance, in both ionic size and chemical hardness. Molecular orbital (MO) calculations using the B3LYP method provided the geometry of **14a** in which two catechols were opposite; however, binding of K^+ (or Li^+) to the spacer –CH_2CH_2–O–CH_2CH_2–O–CH_2CH_2– would fix the flexible conformation of **14a**. As expected, the two catechols formed binding sites of **14a**, which are face to face and close. This provides a new functional chelator for controlling the binding of **14a** with Ln^{3+} in the presence of alkaline metal ions. Finally, this results indicates that chelator **14** is active in displacing the ligand in the solution and a dynamic flexible→rigid equilibrium is produced in K^+ (or Li^+) and Ln^{3+} solutions.

Conclusion

We reported the synthesis and chemical properties of a series of new double-stranded phenylalanine chelators **14** conjugated to catechol. The interactions between double-stranded amino acid chelators (or other ligands) and lanthanide series ions (Ln^{3+}) were discussed using η–χ diagrams as coordinates of electron structure $\mathbf{r}(\chi, \eta)$ based on the chemical hardness theory. According to chemical hardness, **14** is a chemically soft base chelator containing a chemically hard base –CH_2CH_2–O–CH_2CH_2–O–CH_2CH_2– spacer. The diagram suggested that catechol ligand provides stable chelators for Ln^{3+} ions, but not Li^+ and K^+ ions; therefore, **14**–conjugated catechol produced a stable solvated **14**–Ln^{3+} complex. Indeed, binding constants of the **14**–Ln^{3+} complex were 10^4—10^6 M^{-1}. Interestingly, the order of binding stability is identical to the order of the lanthanide contraction effect: $Lu^{3+}<Eu^{3+}<Y^{3+}$. Spectrophotometric titration also provided evidence that the binding constant for Eu^{3+} and **14a** increased in the presence of a chemical hard ion, Li^+ (Na^+ or K^+) (Fig. 5). This result suggested that **14** is ligand displacement active, and that the motion of the molecular skeleton is flexible in solution. Our results indicate the η–χ diagram is a useful tool for developing functional chelators. Further studies of the isolation of the **14**–Ln^{3+} complex and inhibitory effect on cell growth are in progress.

Experimental

General Methods The general approach to the synthesis of the compounds (**11**, **12**) was described in our previous papers.[17,18] The peptide and related ligands were detected on TLC (thin-layer chromatography) plates using iodine vapor or UV (ultraviolet spectrum) absorption. Silica gel column chromatography was performed on silica gel 60N (100 mesh, neutral; Kanto Chemical Co., Japan). Solvent systems were as follows, A: $CHCl_3$–MeOH (20 : 1), and B: $CHCl_3$–MeOH (10 : 1). UV/vis (ultraviolet/visible) spectra were measured with a JASCO V-530 spectrophotometer. pH was measured with a TOA pH instrument (Model HM-60G). Specific rotations were measured with a JASCO DIP-140 digital polarimeter. NMR (nuclear magnetic resonance, as ^{13}C-NMR, ^{1}H-NMR) spectra were obtained with a JEOL α-500 or a Bruker AV300 spectrometer, and NMR samples were dissolved in DMSO-d_6/$CDCl_3$ (volume ratio: 0.5 ml/0.2 ml) with TMS (tetramethylsilane) as an internal reference. FAB-MS (fast atom bombardment mass spectrometry) spectral data were obtained on a JEOL LMS-HX110 spectrometer, and relevant data were tabulated as *m*/*z*.

Synthesis of Bis(Cat-L-Phe)-*N*,*N*-(ethylenedioxy)bis(ethylamine) (14a). Bis(L-Phe)-*N*,*N*-(ethylenedioxy)bis(ethylamine) (12a) CDI (1,1′-carbonyldiimidazole) (4.45 g, 26 mmol) was added to a solution of Boc-L-Phe-OH (5.08 g, 19.2 mmol) in dry $CHCl_3$ (40 ml). The solution was stirred for 1 h at room temperature, 2,2′-(ethylenedioxy)bis(ethylamine) (1.26 g,

8.5 mmol) was added, and the mixture was stirred overnight. This solution was evaporated dry. After the addition of aq. MeOH, the sediment was collected, washed with aq. MeOH, 5% citric acid, 5% $NaHCO_3$, and water, and dried *in vacuo*. The resulting product, bis(Boc-L-Phe)-*N*,*N*-(ethylenedioxy)-bis(ethylamine) (**11a**), a colorless solid, was obtained in 80% yield. The crude product was purified by chromatography on a silica gel column (41 g) and eluted in $CHCl_3$ and 3% MeOH/$CHCl_3$ (stepwise elution); mp 92—94 °C (from MeCN). R*f*(A)=0.37. FAB-MS (nitrobenzylalchohol, NBA) *m*/*z*: 643 $(M+H)^+$.

To **11a** (4.57 g, 5.04 mmol) was added 90% TFA (26 ml). The mixture was stirred for 1 h in an ice bath. After a 5% $NaHCO_3$ and 1 M NaOH workup, product **12a** was extracted with $CHCl_3$, the organic layer was washed with water and dried with dry Na_2SO_4, and **12a** was obtained in 75.0% yield; R*f*(B)=0.16. Oily; ^{1}H-NMR ($CDCl_3$/DMSO-d_6=0.5/0.2) δ: 3.33 (1H, m, $-CH_2-N-$), 3.47—3.50 (1H, m, $-O-CH_2-$), 3.52—3.55 (1H, m, $-CH_2-O-$), 2.69 (1H, dd, *J*=6.9, 8.8 Hz, βH, $-C_6H_5-CH-$), 3.11 (1H, dd, *J*=5.5, 6.9 Hz, βH, $-C_6H_5-C\underline{H}-$), 3.47—3.55 (1H, m, $-C\alpha H-$), 7.19—7.21 (5H, m, aromatic protons), 7.77 (1H, t, *J*=5.5 Hz, –NHaCO–). ^{13}C-NMR ($CDCl_3$/DMSO-d_6=0.5/0.2) δ: 38.63, 41.06, 56.30, 69.48, 69.92, 126.34, 128.28, 129.19, 138.15, and 174.34. FAB-MS *m*/*z*: 443 $(M+H)^+$.

Bis(Cat-L-Phe)-*N*,*N*-(ethylenedioxy)bis(ethylamine) (14a) DEPC (phosphorocyanidate) (0.83 g, 5.1 mmol)[29] was added to a solution of 2,3-bis(benzyloxy)benzoic acid (1.21 g, 3.63 mmol), **12a** (0.697 g, 1.58 mmol), and TEA (triethylamine, 0.4 ml) at 4 °C in dry DMF (20 ml). The mixture was stirred first at 4 °C for 1 h, and then at room temperature overnight. Ice water was added and the solution extracted several times with $CHCl_3$. The combined organic extracts were dried over anhydrous Na_2SO_4 and evaporated dry. The crude residue was chromatographed on silica gel (41 g) with $CHCl_3$ and 3% MeOH/$CHCl_3$ (stepwise elution) as eluents. **13a** was obtained as a colorless solid in 83.0% yield; R*f*(A)=0.66; HR-FAB-MS (NBA) *m*/*z*: 1075.4863 (Calcd for $C_{66}H_{67}N_4O_{10}$ $(M+H)^+$: 1075.4857).

To a solution of **13a** (0.92 g, 0.85 mmol) in MeOH (60 ml) was added 5% Pd–C (0.276 g). The mixture was shaken under a flow of H_2. After the reaction was completed, the catalyst was removed with a glass filter (size G3-4). The filtrate was suspended in ice water and extracted several times with $CHCl_3$. The organic layer was dried with dry Na_2SO_4, filtered, and evaporated. The residue was dried under vacuum to provide **14a** as a pale yellow crystal in 75.3% yield; R*f*(B)=0.48; mp 89—92 °C. $[\alpha]_D^{23}$ −12.0° (*c*=0.00241, EtOH). ^{1}H-NMR ($CDCl_3$/DMSO-d_6=0.5/0.2) δ: 3.40—3.42 (1H, m, $-CH_2-N-$), 3.44—3.49 (1H, m, $-O-CH_2-$), 3.55—3.60 (1H, m, $-CH_2-O-$), 3.11 (1H, dd, *J*=8.9, 13.7 Hz, βH, $-C_6H_5-C\underline{H}-$), 3.20 (1H, dd, *J*=5.5, 7.0 Hz, βH, $-C_6H_5-C\underline{H}-$), 4.82 (1H, m, $-C\alpha H-$), 6.63—6.72 and 6.92—7.29 (3H, m, catechol protons), 7.16—7.29 (5H, m, aromatic protons), 7.80 (1H, t, *J*=5.3 Hz, –NHaCO–) and 8.48 (1H, m, *J*=7.9 Hz, –NHbCO–). ^{13}C-NMR ($CDCl_3$/DMSO-d_6=0.5/0.2) δ: 37.63, 39.08, 54.74, 69.28, 69.94, 117.70 (catecholic C), 118.05 (catecholic C), 118.91 (catecholic C), 126.38, 128.13, 129.19, 137.48, 146.06, 149.26, 169.44, and 171.08. HR-FAB-MS (NBA) *m*/*z*: 715.2968 (Calcd for $C_{38}H_{43}N_4O_{10}$ $(M+H)^+$: 715.2984). FAB-MS (NBA) *m*/*z*: 715 $(M+H)^+$.

Bis(Cat-D-Phe)-*N*,*N*-(ethylenedioxy)bis(ethylamine) (14b) **14b** was prepared in a similar manner to **14a** and obtained as a pale yellow solid in 55% yield; R*f*(B)=0.49. mp 89—92 °C. $[\alpha]_D^{23}$ +13.0° (*c*=0.00249, EtOH). HR-FAB-MS (NBA) *m*/*z*: 715.297 (Calcd for $C_{38}H_{43}N_4O_{10}$ $(M+H)^+$: 715.2981). FAB-MS (NBA) *m*/*z*: 715 $(M+H)^+$.

Bis(benzoyl-L-Phe)-*N*,*N*-(ethylenedioxy)bis(ethylamine) (15a) **15a** was prepared in a similar manner to **13a** and obtained as a colorless solid in 78% yield; R*f*(A)=0.43; mp 185—187 °C. $[\alpha]_D^{23}$ −6.7° (*c*=0.00161, EtOH). ^{1}H-NMR ($CDCl_3$/DMSO-d_6=0.5/0.2) δ: 3.31—3.35 (1H, m, $-CH_2-N-$), 3.38—3.41 (1H, m, $-O-CH_2-$), 3.43—3.50 (1H, m, $-CH_2-O-$), 3.08 (1H, dd, *J*=6.9, 8.8 Hz, βH, $C_6H_5-C\underline{H}-$), 3.20 (1H, dd, *J*=5.8, 7.0 Hz, βH, $C_6H_5-C\underline{H}-$), 4.86 (1H, m, $-C\alpha H-$), 7.13—7.30 (5H, m, $-CO-C_6\underline{H}_5$), 7.35—7.76 (5H, m, $C_6\underline{H}_5-CH_2-$), 7.81 (1H, t, *J*=5.3 Hz, –NHaCO–) and 8.16 (1H, d, *J*=8.0 Hz, –NHbCO–). ^{13}C-NMR ($CDCl_3$/DMSO-d_6=0.5/0.2) δ: 37.80, 39.03, 54.91 (αC), 69.30, 69.98, 126.30, 127.31, 128.07, 129.21, 131.22, 134.13, 137.69, 166.86, and 171.49. HR-FAB-MS (NBA) *m*/*z*: 651.3182 (Calcd for $C_{38}H_{43}N_4O_6$ $(M+H)^+$: 651.3183). FAB-MS (NBA) *m*/*z*: 651 $(M+H)^+$.

Bis(benzoyl-D-Phe)-*N*,*N*-(ethylenedioxy)bis(ethylamine) (15b) Compound **15b** was prepared in a similar manner to **15a** and obtained as a colorless solid in 75% yield; R*f*(A)=0.43. mp 185—187 °C. $[\alpha]_D^{23}$ +7.0° (*c*=0.00298, EtOH). HR-FAB-MS (NBA) *m*/*z*: 651.3165 (Calcd for $C_{38}H_{43}N_4O_6$ $(M+H)^+$: 651.3193).

Circular Dichroism (CD) Measurements The CD spectra of **14a**, **14b**, **15a**, and **15b** were measured on a JASCO J-600 spectrophotometer. Measurements were made along a 1 cm path length in 10 mM HEPES (pH 4.8) in 70% MeCN, with a circular quartz cell at 23±0.1 °C. The CD spectra are shown in Fig. 3 with molar ellipticity, $[\theta]$ $(deg \cdot cm^2 \cdot dml^{-1})$, *versus* wavelength, λ (nm).

Determination of Binding Constants The binding constants (K_b) were obtained by the UV/Vis titration method. Stock solutions of **14a** and lanthanide ions (Ln^{3+}) were prepared in the range of 8.0—8.1×10^{-4} M and 2.5—2.6×10^{-3} M in 10 mM HEPES (70% MeCN, pH 4.8), respectively and were mixed just before recording the spectra. The concentration of **14a** was fixed to **14a**–Y^{3+}: [**14a**]: 8.12×10^{-5} M, [Y^{3+}]: 0.0, 1.5, 3.0, 6.1, 9.1, 15.2, 24.3, 30.4, 45.6, 60.8, 91.2, 121.6, and 152.0×10^{-5} M. **14a**–La^{3+}: [**14a**]: 1.02×10^{-4} M, [La^{3+}]: 0.0, 1.3, 2.5, 5.1, 7.6, 12.7, 20.2, 25.3, 38.0, 50.6, 75.9, 101.2, and 126.5×10^{-5} M. **14a**–Eu^{3+}: [**14a**]: 8.07×10^{-5} mol/l, [Eu^{3+}]: 0.0, 2.6, 5.2, 7.7, 12.9, 20.6, 25.8, 38.7, 51.6, 77.4, 103.2, and 129.0×10^{-5} M. **14a**–Lu^{3+}: [**14a**]: 8.05×10^{-4} M, [Lu^{3+}]: 0.0, 1.3, 2.6, 5.2, 7.7, 12.9, 20.6, 25.8, 38.7, 51.6, 77.4, 103.2, and 129.0×10^{-5} M. **14a**–Eu^{2+}: [**14a**]: 8.05×10^{-5} M, [Eu^{2+}]: 0.0, 1.3, 2.6, 5.2, 7.7, 12.9, 20.6, 25.8, 38.7, 51.6, 77.4, 103.2, and 129.0×10^{-5} M.

Regarding the effect of K^+ ions on the formation of a molecular complex of Eu^{3+} with **14a**, the binding constant of **14a**–Eu^{3+} was obtained using a prepared concentration of [**14a**]: 7.14×10^{-5} M, [K^+]: 7.7×10^{-5} M, and [Eu^{3+}]: 0.0, 1.2, 2.3, 4.6, 7.0, 11.6, 18.6, 23.2, 34.8, 46.4, 69.6, 92.8 and 116.0×10^{-5} M.

Continuous Variation Method Stock solutions of Eu^{3+} (5.74×10^{-4} M) and **14a** (5.74×10^{-4} M) were prepared in 10 mM HEPES (70% MeCN, pH 4.8). Before the measurement, the Eu^{3+} and **14a** solutions were mixed and a standard solution was prepared with a [**14a**/Eu^{3+}] ratio of 0.11, 0.25, 0.43, 0.67, 1.00, 1.50, 2.33, or 4.00. In all the spectra of **14a**–Eu^{3+} complex in each [**14a**/Eu^{3+}] ratio, absorbance (OD) was measured at maximum bands.

Molar Ratio Method Stock solutions of Eu^{3+} (2.34×10^{-4} M) and **14a** (2.34×10^{-4} M) were prepared in 10 mM HEPES (70% MeCN, pH 4.8). To a solution of Eu^{3+} (1.17×10^{-5} M) was added a solution of **14a** (2.34×10^{-4} M) to prepare [**14a**/Eu^{3+}] with a molar ratio of 0.1, 0.2, 0.3, 0.5, 0.8, 1.0, 1.5, 2.0, 3.0, and 5.0. In all spectra of the **15a**–Eu^{3+} complex in each [**14a**/Eu^{3+}] ratio, absorbance (OD) was measured at 340 nm.

Acknowledgments We thank Ms. Tamiko Kiyotani and Mr. Youichi Takase (Showa Pharmaceutical University, Machida, Tokyo, Japan) for NMR and FAB-MS measurements.

References and Notes

1) Anderson C. J., Welch M. J., *Chem. Rev.*, **99**, 2219—2234 (1999).
2) Wu F. B., Han S. Q., Zhang C., He Y. F., *Anal. Chem.*, **74**, 5882—5889 (2002).
3) Bunzli J.-C. G., Piguet C., *Chem. Soc. Rev.*, **34**, 1048—1077 (2005).
4) Heather L. H., Gillies R. J., *Life Sci.*, **77**, 361—371 (2005).
5) Shibazaki M., Sasaki H., Arai T., *Angew. Chem., Int. Ed. Engl.*, **33**, 773—775 (1997).
6) Martínez-Máñez R., Sancenón F., *Chem. Rev.*, **103**, 4419—4476 (2003).
7) Harte A. J., Jensen P., Plush S. E., Kruger P. E., Gunnlaugsson T., *Inorg. Chem.*, **45**, 9465—9474 (2006).
8) Thibon A., Pierre V. C., *Anal. Bioanal. Chem.*, **394**, 107—120 (2009).
9) Steed J. W., Turner D. R., Wallace K. J., "Core Concepts in Supramolecular Chemistry and Nanochemistry," John Wiley & Sons, Ltd., Hoboken, 2007.
10) Anderegg G., Arnaud-Neu F., Delgado R., Felcman J., Popov K., *Pure Appl. Chem.*, **77**, 1445—1495 (2005).
11) Wang C., Seema Choudhary S., Vink C. B., Secord E. A., Morrow J. R., *Chem. Commun.*, **2000**, 2509—2510 (2000).
12) Fricker S. P., *Chem. Soc. Rev.*, **35**, 524—533 (2006).
13) Parr R. G., Pearson R. G., *J. Am. Chem. Soc.*, **105**, 7512—7516 (1983).
14) Pearson R. G., *J. Am. Chem. Soc.*, **107**, 6801—6806 (1985).
15) Parr R. G., Szentpaly L. V., Liu S., *J. Am. Chem. Soc.*, **12**, 1922—1924 (1999).
16) Kobayashi S., Mizushima A., Sasuga A., Watanabe M., *Chem. Pharm. Bull.*, **54**, 761—763 (2006).
17) Kobayashi S., Shinohara H., Tabata K., Yamamoto N., Miyai M., *Chem. Pharm. Bull.*, **54**, 1633—1638 (2006).
18) Kobayashi S., Kobayashi H., Yamaguchi T, Nishida M., Yamaguchi Y., Kurihara M., Miyata N., Tanaka A., *Chem. Pharm. Bull.*, **48**, 920—934 (2000).
19) Kobayashi S., Atuchi N., Wakamatsu H., Hattori M., Kawada A.,

Asano K., *Chem. Pharm. Bull.*, **55**, 1585—1592 (2007).
20) The data of lanthanoide elements from lanthanum (La) to lutetium (Lu) were taken from the www site: <http://en.wikipedia.org/wiki/Lanthanoid>, from Wikipedia, the free encyclopedia, 29 January 2010.
21) Cao X, Li Q, Moritz A, Xie Z, Dolg M, Chen X, Fang W., *Inorg. Chem.*, **45**, 3444—3451 (2006).
22) Hughes I. D., Dane M, Ernst A., Hergert W., Luders M., Poulter J., Staunton J. B., Svane A., Szotek Z., Temmerman W. M., *Nature* (London), **446**, 650—653 (2007).
23) Benesi H. A., Hildebrand J. H., *J. Am. Chem. Soc.*, **71**, 2703—2707 (1949).
24) Liu J.-M., Chen C.-F., Zheng Q.-Y., Huang Z.-T., *Tetrahedron Lett.*, **45**, 6071—6074 (2004).
25) Yoe J. H., Jones A. L., *Ind. Eng. Chem. Anal. Ed.*, **16**, 111—115 (1944).
26) Lindsay E. R., Jakubikova E., Guthrie M. G., Batista E. R., *J. Phys. Chem. A*, **113**, 6745–6750 (2009).
27) Gaussian 03, Revision D.02, Frisch M. J., Trucks G. W., Schlegel H. B., Scuseria G. E., Robb M. A., Cheeseman J. R., Montgomery J. A., Vreven Jr., T., Kudin K. N., Burant J. C., Millam J. M., Iyengar S. S., Tomasi J. Barone V., Mennucci B., Cossi M., Scalmani G., Rega N., Petersson G. A., Nakatsuji H., Hada M., Ehara M., Toyota K., Fukuda R., Hasegawa J., Ishida M., Nakajima T., Honda Y., Kitao O., Nakai H., Klene M., Li X., Knox J. E., Hratchian H. P., Cross J. B., Bakken V., Adamo C., Jaramillo J., Gomperts R., Stratmann R. E., Yazyev O., Austin A. J., Cammi R., Pomelli C., Ochterski J. W., Ayala P. Y., Morokuma K., Voth G. A., Salvador P., Dannenberg J. J., Zakrzewski V. G., Dapprich S., Daniels A. D., Strain M. C., Farkas O., Malick D. K., Rabuck A. D., Raghavachari K., Foresman J. B., Ortiz J. V., Cui Q., Baboul A. G., Clifford S., Cioslowski J., Stefanov B. B., Liu G., Liashenko A., Piskorz P., Komaromi I., Martin R. L., Fox D. J., Keith T., Al-Laham M. A., Peng C. Y., Nanayakkara A., Challacombe M., Gill P. M. W., Johnson B., Chen W., Wong M. W., Gonzalez C., Pople J. A., Gaussian, Inc., Wallingford CT, 2004.
28) Seitz M., Oliver A. G., Raymond N., *J. Am. Chem. Soc.*, **129**, 11153—11160 (2007).
29) Shioiri T., Yokoyama Y., Kasai Y., Yamada S., *Tetrahedron*, **32**, 2211—2217 (1976).